

TERMINAL VELOCITIES FOR A LARGE SAMPLE OF O STARS, B SUPERGIANTS, AND WOLF-RAYET STARS

RAMAN K. PRINJA AND M. J. BARLOW
 Department of Physics and Astronomy, University College London

AND

IAN D. HOWARTH¹

Joint Institute for Laboratory Astrophysics, University of Colorado, and National Institute of Standards and Technology
 Received 1989 November 13; accepted 1990 April 2

ABSTRACT

We argue that easily measured, reliable estimates of terminal velocities for early-type stars are provided (1) by the central velocity asymptotically approached by narrow absorption features and (2) by the violet limit of zero residual intensity in saturated P Cygni profiles. We use these estimators to determine terminal velocities, v_{∞} , for 181 O stars, 70 early B supergiants, and 35 Wolf-Rayet stars. For OB stars our values are typically 15%–20% smaller than the extreme violet edge velocities, v_{edge} , while for WR stars $v_{\infty} = 0.76v_{\text{edge}}$ on average. We give new mass-loss rates for WR stars which are thermal radio emitters, taking into account our new terminal velocities and recent revisions to estimates of distances and to the mean nuclear mass per electron. We examine the relationships between v_{∞} , the surface escape velocities, and effective temperatures.

Subject headings: stars: early-type — stars: winds — stars: Wolf-Rayet

1. INTRODUCTION

The terminal velocity of a stellar wind, v_{∞} , is defined as the velocity of outflowing matter at large distances from the star, where it is no longer experiencing significant acceleration but is not yet interacting significantly with the interstellar medium. Reliable estimates of v_{∞} are needed for several reasons. The theory of radiation pressure-driven winds makes important predictions concerning the relationship between the terminal velocity and the photospheric escape velocity (Abbott 1978). Terminal velocities are needed for the determination of mass-loss rates, \dot{M} , derived, for example, from modeling UV resonance line profiles (where $\dot{M} \propto v_{\infty}^2$) or from radio measurements of the free-free radiation from the winds ($\dot{M} \propto v_{\infty}$). Knowledge of wind terminal velocities is also needed for the application of theories for the interaction between stellar winds and the interstellar medium.

Since the time of the first large-scale ultraviolet spectroscopic survey of the mass-loss characteristics of luminous OB stars (Snow and Morton 1976), the terminal velocity of a stellar wind has normally been observationally defined as the modulus of the largest negative velocity seen in absorption in the P Cygni profiles of UV resonance lines. Examples of this blue absorption edge velocity are shown in Figure 1. (We use v_{edge} to signify the edge velocity observed in a given line and v_{max} to denote the maximum edge velocity in any line.) However, even presuming that the optical depth in the line is sufficient for it to be detectable at large radii, this operational definition will be correct only if there are no significant line broadening mechanisms other than the macroscopic Doppler broadening brought about by the bulk velocity field. The observation of P Cygni profiles showing extended regions of zero residual intensity and blue wings with finite width throw the applicability of this condition into question.

Models of saturated P Cygni profiles using the Sobolev approximation and incorporating velocity laws which increase

monotonically with radius (e.g., Castor and Lamers 1979) predict that zero intensity should be reached only at v_{∞} and that the profiles should return sharply to unit continuum intensity (since the forward-scattering halo contains material at all projected line of sight velocities up to, but excluding, the terminal velocity). Observed saturated profiles instead often show an extended absorption region which is black, i.e., has zero residual intensity within observational uncertainties, while a finite absorption region between the shortward edge of the black absorption core (v_{black}) and the velocity v_{edge} at which the profile intersects the continuum level is normal (see Fig. 1). These effects are consistent with nonmonotonic wind velocity laws, as first shown by Hamann (1980, 1981), who parameterized the required local velocity fields by large random microturbulent motions, and by Lucy (1982, 1983), who adopted large numbers of forward-propagating shocks resulting from instabilities in the flows as a specific physical model. The recent numerical modelling of radiatively driven non-laminar stellar winds by Owocki, Castor and Rybicki (1988, hereafter OCR) predicts that *reverse* shocks in the flow should lead to the highest velocity material being located in rarefaction zones, so that the small amount of material with velocities much higher than the terminal flow speed should cause a residual amount of absorption on the blue edge. An implication of Lucy's model (and of OCR's, but in the context of a more realistic physical structure) is that v_{max} can exceed v_{∞} by an amount related to the amplitude of shocks in the wind, and thus, as discussed by Abbott (1985), v_{black} should provide a better estimate of the wind terminal velocity than does v_{max} .

In addition to these effects, discrete absorption components are commonly found within the absorption troughs of unsaturated P Cygni resonance line profiles seen in the UV spectra of luminous OB stars, occurring at the same velocity in different ions (Morton 1976; Snow 1977; Lamers, Gathier, and Snow 1982; Prinja and Howarth 1986). Howarth and Prinja (1989) have shown that the available data are consistent with the hypothesis that the mechanism responsible for discrete com-

¹ 1988–1989 JILA Visiting Fellow.

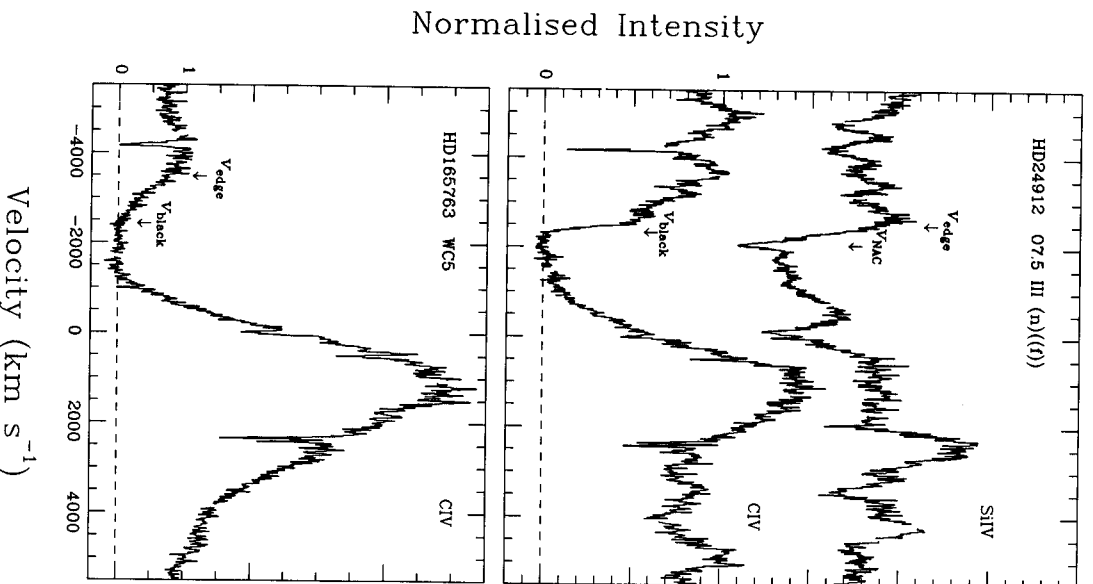


FIG. 1.—Examples of the principal stellar wind velocity measurements made on the UV resonance line profiles of O and WR stars.

ponents operates in *all* O stars. An example of discrete absorption features in the Si IV spectrum of HD 24912 is shown in Figure 1.

Recent investigations of short-term (hours–days) variability in the UV P Cygni profiles of selected O stars have shown that the velocities of discrete absorption components have a systematic time dependence (Prinja, Howarth, and Henrichs 1987; Prinja 1988; Prinja and Howarth 1988). These studies show that the discrete components first appear as broad optical depth enhancements ($\Delta v \simeq 0.5v_{\max}$) at $\sim 0.5v_{\max}$ and evolve into high-velocity narrow absorption components (NACs; $\Delta v_{\text{NAC}} \simeq 0.1v_{\max}$) with central velocities v_{NAC} which asymptotically approach $\sim 0.85v_{\max}$ (Howarth and Prinja 1989). The time scale for this velocity evolution appears to be proportional to the rotation period of the star (Prinja 1988). While more than one set of discrete absorption components may be visible in the spectrum of a star at any one time, a single “snapshot” UV spectrum will usually show a narrow absorption component at $v_{\text{NAC}} \sim 0.8v_{\max}$. It has been proposed by Prinja and Howarth (1986), by Henrichs, Kaper, and Zwartthoed (1988), and by Howarth and Prinja (1989) that the final

central velocity of the discrete absorption components, $v_{\text{NAC}}(t \rightarrow \infty)$, also provides a better indicator of v_{∞} than does v_{\max} .

In this paper we will argue that measurements of both black absorption edge velocities and of narrow absorption component velocities give consistent estimates of wind terminal velocities and that either diagnostic may be used in isolation in a straightforward manner to estimate v_{∞} . Using high-resolution *IUE* spectra, we then go on to measure wind terminal velocities for 181 O stars, for 70 B0–B3 supergiants, and for 35 Wolf-Rayet (WR) stars.

II. OBSERVATIONAL INDICATORS OF v_{∞}

The discrete absorption components observed in unsaturated P Cygni profiles represent an optical depth enhancement at some specific velocity in the wind, associated with material having a finite velocity dispersion. We interpret the maximum velocity of these features (the narrow components) as the terminal velocity, with the difference $v_{\text{edge}} - v_{\infty}$ arising from a *local* velocity field, which has been parameterized as “microturbulence” by Hamann (1980, 1981), and by Groenewegen, Lamers, and Pauldrach (1989). A physical interpretation of this microturbulence is offered by the work of Owocki, Castor, and Rybicki (1988), who found that their unstable time-dependent wind models are able to produce discrete absorption components that are stable over all phases of the chosen driving wave period of 4000 s. In the OCR model, the discrete components are due to the superposition of the absorption by density enhancements in the wind that are bounded on their inner edges by strong reverse shocks. Figure 12 of Owocki, Castor, and Rybicki reveals the highest velocity narrow absorption component predicted by their model to be at exactly the wind terminal velocity. The work of Prinja (1988) has shown that the time scale for evolution of discrete absorption components appears to be directly related to the stellar rotation period, with fast rotators like 68 Cyg and ξ Per showing much more rapid velocity evolution of the discrete absorption components than slow rotators like 19 Cep and HD 162978. Eventually, an outward-moving density enhancement will reach a velocity comparable to the terminal flow speed, and the absorption due to it will merge with that produced by other density enhancements farther out in the wind that are asymptotically approaching this velocity.

The narrow components are observed to evolve toward increasing velocity with time. We therefore conclude that $v_{\text{NAC}}(t \rightarrow \infty)$ provides a good indicator of v_{∞} ; however, estimating this quantity observationally requires frequent (\sim hourly) *IUE* spectra taken over a sufficiently extensive period (\sim days), and such data are only available for a very few stars. It is therefore desirable to find a means to estimate v_{∞} from a single “snapshot” UV spectrum. As shown by Howarth and Prinja (1989), this can be done, since the width of a discrete component decreases as its central velocity increases (i.e., as it evolves into a “narrow component”), an appropriate combination of the two should be approximately constant, and equal to $v_{\text{NAC}}(t \rightarrow \infty)$. From the time sequence data of Prinja, Howarth, and Henrichs (1987; ξ Per), Prinja and Howarth (1988; 68 Cyg), and Prinja (1988; 19 Cep, HD 162978), we confirm that the central velocity of the narrow absorption components, v_{NAC} , plus the half-width at half-maximum depth of the model Doppler profiles fitted to them, HWHM_{NAC} , is approximately constant and equal to $v_{\text{NAC}}(t \rightarrow \infty)$ during the time that the discrete absorption components are identifiable

in isolated spectra, i.e., when they are present as narrow absorption features. (We define \bar{v}_{NAC} as the mean central velocity of the narrow components measured in all resonance line profiles in a given spectrum, taking into account only the most violet-shifted feature when multiple components are visible in a given line.)

To illustrate this, the central velocities of consecutive sequences of discrete absorption components in the spectra of 68 Cyg and 19 Cep are plotted in Figure 2 as a function of time (data from Prinja and Howarth 1988 and Prinja 1988). The sum $\bar{v}_{\text{NAC}} + \text{HWHM}_{\text{NAC}}$ is also shown and is seen to be a good approximation to the velocity asymptotically approached by the narrow components. The time scale for the development and recurrence of the discrete features is a few days for the relatively rapid rotator 68 Cyg ($v_e \sin i = 315 \text{ km s}^{-1}$; Uesugi and Fukuda 1982), whereas for the slow rotator 19 Cep ($v_e \sin i = 40 \text{ km s}^{-1}$) it is much longer.

Also plotted in Figure 2 are the values of v_{black} derived from the saturated C IV profiles. It is clear that v_{black} can be identified with the asymptotic value of \bar{v}_{NAC} measured from long time sequences of data, at least for O stars. In fact, v_{black} is very

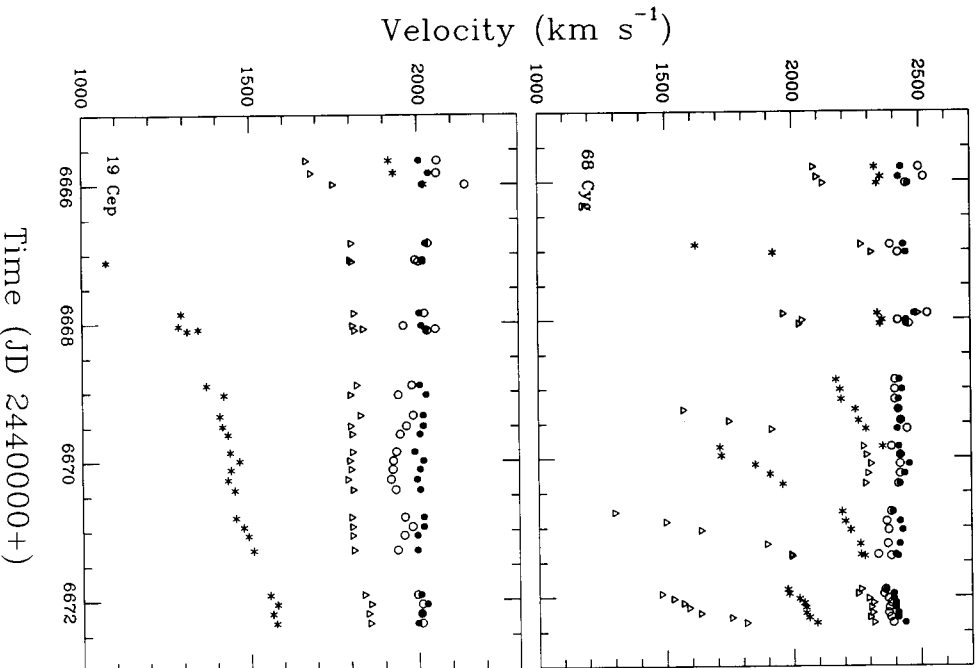


FIG. 2.—Central velocities of consecutive sequences of variable opacity enhancements in 68 Cyg (HD 203064) and 19 Cep (HD 209975) as a function of time. The sum $\bar{v}_{\text{NAC}} + \text{HWHM}_{\text{NAC}}$ (for the most blueshifted component) is also shown (open circles), together with the corresponding values of v_{black} derived from the C IV profiles (filled circles).

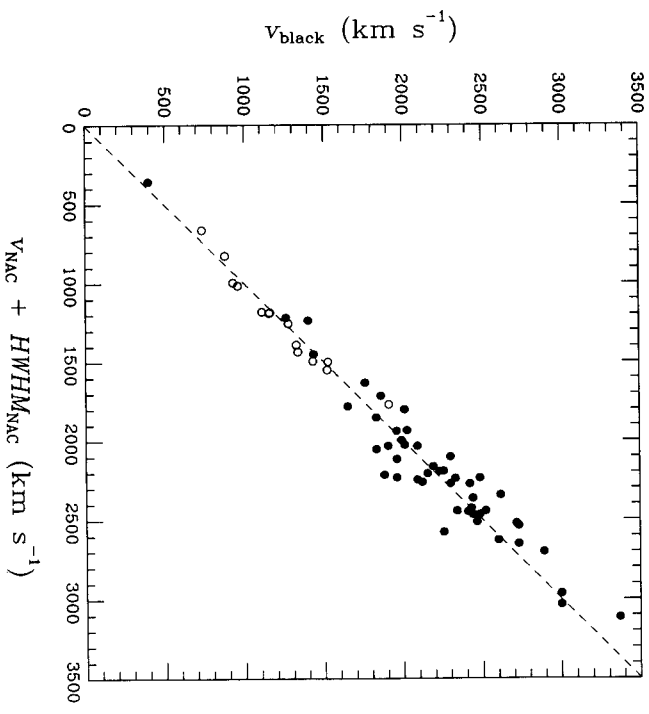


FIG. 3.—A comparison of v_{black} , estimated from individual C IV profiles of O stars (filled circles) and B supergiants (open circles), and the corresponding sum of $\bar{v}_{\text{NAC}} + \text{HWHM}_{\text{NAC}}$. The dashed line shows a one-to-one correspondence.

stable, showing significantly less variation than the sum $\bar{v}_{\text{NAC}} + \text{HWHM}_{\text{NAC}}$, as well as being a more straightforward measurement to make. Hence it is potentially the most direct observational indicator of v_{∞} .

Among our total sample, 48 O stars and 13 B supergiants possess both saturated C IV profiles from which v_{black} can be measured and unsaturated Si IV profiles from which narrow component velocities and HWHM_{NAC} can be measured. Figure 3 is a plot of v_{black} versus $\bar{v}_{\text{NAC}} + \text{HWHM}_{\text{NAC}}$ for these stars (cf. Fig. 10 of Howarth and Prinja 1989). The dashed line corresponds to a 1:1 correlation, which the data fit very tightly (the product-moment correlation coefficient is $r = 0.98$).

The results presented here, and in Howarth and Prinja (1989), therefore show that, for OB stars, v_{black} and $\bar{v}_{\text{NAC}} + \text{HWHM}_{\text{NAC}}$ measure the same quantity, which we have identified with v_{∞} . Since v_{black} is the simpler measurement and the more stable quantity, we preferentially adopt $v_{\infty} = v_{\text{black}}$ for stars showing saturated P Cygni lines; C IV $\lambda 1550$ nearly always provides the most easily measured profile. For stars without saturated profiles, but with readily identifiable narrow absorption components in an individual spectrum, we adopt $v_{\infty} = \bar{v}_{\text{NAC}} + \text{HWHM}_{\text{NAC}}$.

The conclusion that, for saturated line profiles, the velocity range for black absorption extends as far as the wind terminal velocity but no further probably has a physical interpretation in that material moving at velocities in excess of the terminal flow speed is extremely rarefied (OCR). Interestingly, therefore, for saturated profiles the terminal velocity is given by the velocity where the black absorption starts to return to the continuum, just as in classical laminar flow Sobolev models.

III. RESULTS

a) O Stars and B Supergiants

Table 1 gives measurements of v_{max} , v_{black} , and \bar{v}_{NAC} for 181 O stars which have a saturated P Cygni profile and/or identi-

TABLE 1
STELLAR WIND VELOCITIES FOR O STARS

HD/BD/ CPD	Spectral Type	v_{max} (km s ⁻¹)	v_{black} (km s ⁻¹)	\bar{v}_{NAC} (km s ⁻¹)	v_{∞} (km s ⁻¹)
108.....	O6: fType	2700	1960	1975	1960
1337.....	O9 III: (n)	2400	...	1840	1960
5005A.....	O6.5 V (f)	3350	...	2655	2835
12323.....	ON9 V	1630	...	950	1105
12993.....	O6.5 V	2750	...	2185	2290
13268.....	O7	2370	...	1910	2070
13745.....	O9.7 II (n)	2400	1905	1920	1905
14434.....	O5.5 V n(f)p	2300	1960	1805	1960
14633.....	ON8 V	2100	...	1580	1690
14947.....	O5 I f+	2550	1885	...	1885
15137.....	O9.5 II-III (n)	2000	...	1530	1640
15558.....	O5 III (f)	3200	2735	...	2735
15570.....	O4 I f+	3200	2605	...	2605
15629.....	O5 V (f)	3200	2810	...	2810
15642.....	O9.5 III: n	1800	1435	...	1435
17505.....	O6.5 V (f)	2800	...	1230	2160
19820.....	O8.5 III (n)	2650	2255	2000	2255
24912.....	O7.5 III (n)(f)	2500	2330	2130	2330
30614.....	O9.5 Ia	1900	1590	...	1590
34656.....	O7 II (f)	2500	2155	2020	2155
35619.....	O7 V	2450	...	1775	1870
35921.....	O9.5 III: n	2300	1990	1825	1990
36486.....	O9.5 II	2300	...	1850	1995
36861.....	O8 III (f)	2650	...	2015	2125
36879.....	O7 V (n)	2400	...	2110	2170
37022.....	O6-O4 P var	1000	...	350	510
37043.....	O9 III	2450	...	2070	2195
37742.....	O9.7 Ib	2250	1860	1620	1860
39680.....	O6 V: [n]pe var	1800	...	1540	1635
41161.....	O8 V n	2400	...	1950	2035
42088.....	O6.5 V	2215	...	2020	2155
46056.....	O8 V n	1500	...	1200	1305
46150.....	O5 V (f)	3150	...	2780	2925
46223.....	O4 V (f)	3100	2910	...	2910
46485.....	O7 V n(e)	2250	...	1730	1780
46966.....	O8 V	2215	...	1945	2105
47129.....	O8 P	2645	...	2255	2410
47432.....	O9.7 Ib	2000	1590	...	1590
47839.....	O7 V (f)	2600	...	1925	2055
48099.....	O7 V	3300	...	2840	2925
48279.....	O8 V	1700	...	1515	1635
53975.....	O7.5 V	2025	...	1705	1795
54662.....	O6.5 V	2750	...	2265	2395
57060 ^a	O7 Ia: fp var	2135	1425	...	1425
57061.....	O9 II	2350	1960	2000	1960
58509.....	O8 V	1500	...	1165	1250
60369.....	O9 III	2300	...	1725	1825
60848.....	O8 V	1850	...	1620	1720
61347.....	O9 I	2300	1775	...	1775
63005.....	O6 V	2450	2120	2045	2120
66811.....	O4 I (n)f	2700	2485	2215	2485
68450.....	O9.7 Ib-II	2150	...	1905	1950
69464.....	O6.5 Ib (f)	2600	2300	2035	2300
69648.....	O8.5 I	2700	2090	2055	2090
73882.....	O8.5 V (n)	2550	...	2205	2315
74194.....	O8.5 Ib (f)	2550	2160	...	2160
74920.....	O8	2800	...	2365	2425
75222.....	O9.7 Ia b	2250	1840	...	1840
75759.....	O9 V n	1400	...	1170	1245
76341.....	O9 I	2250	...	1450	1500
76968.....	O9.7 Ib	2400	1815	...	1815
90273.....	O7	2500	...	2140	2240
91572.....	O6 V (f)	2650	2410	2245	2410
91651.....	O9 V: n	1900	...	1600	1705
91824.....	O7 V (f)	2700	...	2240	2270
92554.....	O9.5 II	1750	1260	1035	1260
92850.....	O9.5 I	1900	...	1530	1615

610

TABLE 1—Continued

HD/BD/ CPD	Spectral Type	v_{\max} (km s ⁻¹)	v_{back} (km s ⁻¹)	\bar{v}_{NAC} (km s ⁻¹)	v_{∞} (km s ⁻¹)
93129A.....	O3 I f	3950	3150	...	3150
93130.....	O6 III (f)	3100	2390	...	2390
93146.....	O6.5 V (ff)	2975	...	2400	2565
93204.....	O5 V (ff)	3250	2890	2530	2890
93205.....	O3 V	3630	3370	2845	3370
93206.....	O9.7 Ib: (n)	2350	1400	1020	1400
93222.....	O7 III (ff)	3050	...	2550	2645
93249.....	O9 III	2200	...	1685	1755
93250.....	O3 V (ff)	3350	...	3000	3160
93403.....	O5 III (f) var	2750	2615	2205	2615
93521.....	O9 V	1075	400	190	400
93843.....	O5 III (f) var	3150	2730	2405	2730
96715.....	O4 V (ff)	3430	3000	2845	3000
96917.....	O8.5 Ib (f)	2550	2000	...	2000
96946.....	O6 V:	2770	2465	2300	2465
99546.....	O8	2400	...	2070	2205
100213.....	O8.5 V n	1800	...	1530	1625
100444.....	O9 I	2600	...	2005	2090
101131.....	O6 V (ff)	3300	...	2535	2690
101190.....	O6 V (ff)	3100	...	2775	2945
101205.....	O7 III n(f)	3200	...	2500	2665
101298.....	O6 V (ff)	3300	2740	...	2740
101413.....	O8 V	2400	...	2095	2230
101436.....	O6.5 V	3100	2600	2490	2600
105056.....	ON9.7 Ia e	1325	680	...	680
105627.....	O9 II-III	2400	...	1830	1935
112244.....	O8.5 Iab (f)	2250	1575	...	1575
112784.....	O9.5 III	1650	...	1180	1275
113904.....	O9 II	2850	2255	2460	2255
115455.....	O7.5 III (ff)	2800	...	2100	2210
116852.....	O9 III	2600	2230	2035	2230
123008.....	ON9.7 Iab	2300	1250	...	1250
124314.....	O6 V (n)(ff)	2700	...	2260	2425
124979.....	O8.5	3400	...	2685	2775
135240.....	O7.5 III (ff)	2700	...	2230	2390
135591.....	O7.5 III (ff)	2450	...	2055	2180
148937.....	O6.5 f?p	2650	...	2055	2215
149038.....	O9.7 Iab	2200	1830	1715	1830
149404.....	O9 Ia	2850	2450	...	2450
149757.....	O9 V	1640	...	1385	1470
150136.....	O5 III: n(f)	3700	3160	...	3160
151515.....	O7 II (f)	2800	2520	2230	2520
151804.....	O8 Ia f	2250	1445	...	1445
152218.....	O9.5 IV (n)	2125	...	1925	2020
162233.....	O6 III: (fp)	3200	2730	2345	2730
152246.....	O9 III-IV (m)	2200	...	1610	1670
152247.....	O9.5 II-III	2800	...	2100	2235
152248.....	O7 Ib: (n)(fp)	2700	2420	2040	2420
152249.....	OC9.5 Iab	2350	2010	1610	2010
152405.....	O9.7 Ib-II	2200	...	1750	1825
152408.....	O8: Ia fpe	2200	955	...	955
152424.....	OC9.7 Ia	2175	1760	1495	1760
152590.....	O7.5 V	2150	...	1650	1745
152623.....	O7 V (n)(ff)	3300	...	2830	3015
152723.....	O6.5 III (f)	3500	3000	2835	3000
153426.....	O9 II-III	2350	...	2065	2160
153919.....	O6.5 Ia f+	2650	1820	...	1820
154368.....	O9.5 Iab	2200	1850	...	1850
155806.....	O7.5 V [n]e	2900	...	2230	2390
156292.....	O9.5 III	1530	...	1235	1320
156359.....	O9 III	2175	...	1800	1885
157857.....	O6.5 III (f)	3050	2300	2150	2300
159176.....	O7 V + O7 V	3000	...	2475	2555
162978.....	O7.5 II (ff)	2800	2350	...	2350
163758.....	O6.5 Ia f	2675	2420	...	2420
163892.....	O9 IV (m)	1575	...	1285	1370
164492.....	O7.5 III (ff)	1700	...	1495	1580
164794.....	O4 V (ff)	3550	2750	...	2750

PRINJA, BARLOW, AND HOWARTH

TABLE 1—Continued

HD/BD/ CPD	Spectral Type	v_{\max} (km s ⁻¹)	v_{black} (km s ⁻¹)	\bar{v}_{NAC} (km s ⁻¹)	v_{∞} (km s ⁻¹)
165052.....	O6.5 V (n)(f)	2800	...	2205	2295
167263.....	O9.5 II–III (tn)	2450	...	2025	2155
167264.....	O9.7 Iab	2100	...	1735	1795
167659.....	O7 II (f)	2730	2440	2135	2440
167771.....	O7 III: (n)(f)	2700	2485	2320	2485
167971.....	O8 Ib (fp)	2275	2185	...	2185
168075.....	O6 V (f)	3200	2845	...	2845
168076.....	O4 V (f)	3550	3305	...	3305
168941.....	O9.5 II–III	2250	...	1665	1755
171589.....	O7 II (f)	3200	2935	...	2935
175754.....	O8 II (f)	2700	2060	...	2060
175876.....	O6.5 III: (n)(f)	2900	2430	2260	2430
186980.....	O7.5 III: (f)	2550	...	2070	2205
188001.....	O7.5 Ia f	2330	1980	...	1980
188209.....	O9.5 Iab	2100	1650	1470	1650
190429A.....	O4 I f+	2850	1880	2020	1880
190864.....	O6.5 III: (f)	2800	2440	2250	2440
191423.....	O9 III: n	1350	...	750	800
192639.....	O7 Ib (f)	2700	2180	...	2180
193322.....	O9 V: (tn)	1800	1605
193443.....	O9 III	2500	...	2090	2250
193514.....	O7 Ib (f)	2750	2190	2055	2190
199579.....	O6 V (f)	3300	2715	2275	2715
201345.....	ON9 V	1550	...	1280	1380
202124.....	O9.5 Iab	2100	1820	...	1820
203064.....	O7.5 III: n(f)	2800	2340	2310	2340
206267.....	O6.5 V (f)	3225	...	2535	2680
207198.....	O9 Ib–II	2450	2090	1905	2090
209481.....	O9 V:	2250	...	1815	1925
209975.....	O9.5 Ib	2400	2010	1835	2010
210809.....	O9 Iab	2750	2135	...	2135
210839.....	O6 I (n)fp	2600	2300	...	2300
214680.....	O9 V	1375	...	1075	1120
215835.....	O6 V (n)	3275	2810	...	2810
217086.....	O7 V n	3000	2510	...	2510
218195.....	O9 III	2300	...	1895	1985
218915.....	O9.5 Iab	2425	1830	1895	1830
223673.....	O6.5 V	2800	2485	...	2485
242908.....	O4 V (n)	3200	...	2645	2785
303308.....	O3 V (f)	3300	3035	...	3035
+34°1058...	O8	2315	2025	1860	2025
+60°594...	O9 V	1550	2035	1435	2035
+60°2522...	O6.5 (n)fp	2600	2035
+59°2600...	O6 V (f)	3400	...	2940	3065
+59°2603...	O7 V (f)	2050	...	1695	1795
+59°2641...	O5 V	3200	2870	...	2870

* See text, § III,4, for a discussion of the data sources for this star.

fiable narrow components. With only one exception,² these data are reproduced from Howarth and Prinja (1989, where they are respectively denoted as v_* , v_b , and v_c), who give details of data reduction techniques and procedures used for modeling the discrete absorption components, as well as primary sources

² The exception is HD 57060 (= UW CMA), for which the value of v_{black} (= v_{∞}) listed in Table 1 is 400 km s⁻¹, larger than that listed by Howarth and Prinja (1989). Significant variations in the C IV profile of this system occur during its 4.39 day orbital cycle (Heap 1982). The terminal velocity of 1425 km s⁻¹ listed in Table 1 was measured from SWP 3390, which corresponds to phase 0.573 (Stickland 1989), with the O7 Ia:fp primary in front. On SWP 9620 (phase 0.071; secondary in front) v_{black} = 1025 km s⁻¹ was measured from the C IV profile; we consider that this value is likely to reflect the terminal velocity of the secondary star, for which a spectral type of O9.5 V–B0 V has been inferred indirectly (van Genderen *et al.* 1988). We also note that some of the terminal velocities derived for other spectroscopic binaries in our sample could be affected by orbital motions of up to ~200 km s⁻¹.

for the adopted spectral types. The final column of Table 1 lists the adopted values of v_{∞} , which correspond to v_{black} for stars having saturated lines (C IV in all cases except the five ON stars, for which N V was used), and to \bar{v}_{NAC} + HWHM_{NAC} , otherwise. The velocities have measurement errors estimated to be $\lesssim 100$ km s⁻¹.

Corresponding results for 70 B supergiant stars having spectral types of B3 or earlier are listed in Table 2. Spectral types were again taken from the primary sources listed by Howarth and Prinja (1989), supplemented where necessary by classifications from Hiltner (1956), Lesh (1968), and Morgan, Code, and Whitford (1956). We restrict ourselves to B0–B3 supergiants in the knowledge that the C IV resonance line still provides a sensitive diagnostic of mass loss for these stars (e.g., Heck *et al.* 1984; Walborn and Nichols-Boblin 1987). As for the bulk of the O stars, the values of v_{edge} and v_{black} listed in

TABLE 2
STELLAR WIND VELOCITIES FOR B SUPERGIANTS

HD	SWP	Spectral Type	v_{esc}^a (km s ⁻¹)	v_{edge}^1 (km s ⁻¹)	v_{black}^1 (km s ⁻¹)	\bar{v}_{MAC}^1 (km s ⁻¹)	v_{∞}^1 (km s ⁻¹)
2905.....	14902	BC0.7 Ia	557	1345	1105	...	1105
5045.....	9334	B3 Ia	(400)	565	405	...	405
13854.....	2737	B1 Ia	(513)	1105	920	...	920
14143.....	9435	B2 Ia	376	1005	645	...	645
14818.....	9416	B2 Ia	407	820	565	...	565
24398.....	6454	B1 Ib	522	1335	...	1215	1270
29138.....	10051	B1 Ia	(531)	1300	...	1140	1315
37128.....	(PH86) ^b	B0 Ia	700	1980	1910	1725	1910
38771.....	(PH86) ^b	B0.5 Ia	580	1800	1525	1425	1525
40111.....	18943	B1 Ia	663	1560	...	1340	1465
41117.....	4374	B2 Ia	399	850	510	...	510
43384.....	4656	B3 Ia	442	715	...	600	710
47420.....	9895	B1 Ib	(558)	1250	960	885	960
52382.....	27404	B1 Ib	(558)	1245	900	...	900
53138.....	13564	B3 Ia	431	845	...	750	830
58510.....	21677	B1 Ia	(531)	1375	930	910	930
77581.....	22301	B0.5 Ia	(590)	1310	1105	...	1105
86606.....	14677	B1 Ib	(558)	615	...	420	490
91316.....	(PH86) ^b	B1 Ia	(531)	1350	1110	1090	1110
91452.....	20622	B0 Ia	(713)	2095	1635	...	1635
91943.....	23760	B0.5 Ib	(558)	1690	...	1255	1405
91969.....	9076	B0 Ia	(713)	1785	1545	...	1545
92964.....	6316	B2.5 Ia	(410)	880	435	...	435
93840.....	21525	B2 Ib	(416)	1255	...	995	1160
94493.....	21505	B0 Ia	(702)	1545	...	1345	1495
94909.....	14810	B0 Ia	(713)	1250	1050	...	1050
96248.....	7702	BC1.5 Ia	(440)	880	675	...	675
97522.....	31295	B1.5 Ib	(436)	1300	...	1040	1190
97707.....	31272	B2 Ib	(416)	1050	870	...	870
99857.....	22170	B0.5 Ib	(558)	1720	...	1600	1705
99953.....	9074	B1.5 Ia	(444)	805	510	...	510
100276.....	22147	B1 Ib	(558)	1830	1430	...	1430
104683.....	22169	B1 Ib	(558)	1345	...	1020	1145
106343.....	6320	B1.5 Ia	(444)	1275	795	...	795
109399.....	20308	B0.5 Ia	(558)	1565	1325	...	1325
109867.....	14928	B0.7 Ib	(558)	1635	1155	...	1085
113012.....	22168	B0.2 Ib	(625)	1445	...	1075	1215
115842.....	27405	B0.5 Ia	(590)	1530	1180	...	1180
116084.....	6322	B2.5 Ib	(467)	1040	550	...	550
119608.....	5647	B1 Ib	(558)	1120	880	...	880
148379.....	4349	B1.5 Ia	(444)	685	510	...	510
148422.....	23529	B0.5 Ia	(590)	2185	1335	...	1335
148688.....	1871	B1 Ia	(513)	870	725	...	725
150898.....	9267	B0.5 Ia	(590)	1310	1300
152235.....	16205	B0.5 Ia	(590)	1445	850	...	850
152236.....	15267	B1.5 Ia ⁺	441	675	390	...	390
152667.....	(H84b) ^c	B0 Ia(n)	(590)	1565	795	...	795
154090.....	14828	B1 Ia	554	1305	915	...	915
155985.....	7742	B0.5 Ia	(590)	1280	...	1190	1225
157038.....	30759	B3 Ia	(442)	1015	525	...	525
157246.....	(PH86) ^b	B1 Ib	(558)	1000	735	...	735
160993.....	23541	B1 Ia	(513)	1375	...	1200	1320
163181.....	2235	BNO.5 Ia	(590)	885	520	...	520
163522.....	32073	B1 Ia	(513)	1490	1240	...	1240
164402.....	18147	B0 Ib	658	2115	...	1585	1650
165024.....	6331	B2 Ib	(416)	1130	...	1000	1130
167264.....	6490	B0 Ia	732	2020	1640	...	1640
167402.....	23528	B0 Ib	(691)	2185	...	1905	2005
167756.....	30453	B0.5 Ia	(590)	2285	...	1700	1865
178487.....	26986	B0 Ia	(713)	1660	...	1430	1520
179407.....	23833	B0.5 Ib	(558)	1670	...	1470	1585
185859.....	14207	B0.5 Ia	(590)	2135	...	1455	1715
190066.....	18310	B1 Ia	(531)	1570	1275	1155	1275
190603.....	14942	B1.5 Ia ⁺	452	670	485	...	485
191877.....	14825	B1 Ib	(558)	1310	1160	1020	1160
198478.....	13907	B3 Ia	393	655	470	...	470
204172.....	6481	B0 Ib	644	2015	...	1500	1630
206165.....	6336	B2 Ib	416	910	640	...	640
213087.....	2736	B0.5 Ib	552	1595	1520	1470	1520
235783.....	21706	B1 Ib	(558)	1305	1070	...	1070

^a Values in parentheses are means for the spectral type.

^b Data from Pinijn and Howarth 1986.

^c Measurements from the mean spectrum constructed by Howarth 1984b.

Table 2 were determined from the C IV profiles, while the values of \bar{v}_{NVC} represent the mean values found from unsaturated C IV, Si IV and N V resonance line profiles. Narrow components may be present in other lines (e.g., HD 152667 shows such features in C II $\lambda 1335$ and Fe III $\lambda 1900$; Howarth 1984a, b), but we have not carried out a systematic study of their occurrence.

The sample represents all of the B0–B3 supergiants which had high-resolution *IUE* spectra available from the Rutherford Appleton Laboratory World Data Centre archive at the time of our investigation (mid-1989). Prinja (1989) examined the UV spectra of normal nonsupergiant B0–B5 stars and found no evidence of narrow absorption components or of saturated stellar wind profiles; the wind terminal velocities of these stars cannot, therefore, be safely determined from direct measurement of *IUE* data.

Table 3 lists the mean terminal velocities found for each spectral type in luminosity classes I, III, and V in our sample. (We ignored “f” qualifiers and omitted the extreme B1⁺ supergiants and the OBNC stars from these means, together with HD 93521, which has very peculiar profiles—see Prinja and Howarth 1986.) Table 3 shows that, for spectral types running from O4 to O9.5, the mean terminal velocities decline quite steeply for the dwarfs and giants, falling from 3000 km s^{−1} to 1400 km s^{−1} and from 2800 km s^{−1} to 1500 km s^{−1}, respectively, while for the supergiants the decline is much less steep (from 2300 km s^{−1} to 1800 km s^{−1}). The mean terminal velocities of the B supergiants continue this decline, falling from 1600 km s^{−1} at B0 to 600 km s^{−1} at B3.

b) Wolf-Rayet Stars

Figure 1 shows the C IV profile observed in the spectrum of the WC5 star HD 165763. The velocity corresponding to the black absorption edge, v_{black} , is marked, as is our estimate for the position of v_{edge} . Determining the position of v_{edge} is often

difficult in O star spectra because of the need to estimate where unit continuum lies; in WR spectra, with their many blended emission lines, it can be even more of a problem. By contrast, the determination of v_{black} is straightforward, as Figure 1 shows. We assume that, as for the O stars, it provides a reliable measurement of v_{∞} ; this assumption is justified by the comparisons with other indicators of v_{∞} discussed in § IIIc.

Thirty-five Galactic Wolf-Rayet stars had well-exposed high-resolution *IUE* spectra available in the Rutherford Appleton Laboratory World Data Centre archive at the time of our investigation. The velocity measurements made from these spectra are presented in Table 4. For the single WN stars in our sample, the N V resonance line always exhibits a saturated absorption profile, as does the C IV resonance doublet for all but the WN3 star; Si IV shows saturated absorption for the WN6–WN8 types. The subordinate lines He II $\lambda 1640$ and N IV $\lambda 1718$ almost never reach zero intensity.

For the single WC stars, the C IV and Si IV resonance lines always have saturated absorption, as do the C II resonance line profiles for all but the WC5 types. The absorption profiles of the C III $\lambda 1175$ and $\lambda 1247$ subordinate lines always reach zero intensity in the spectra of the single WC stars, whereas the absorption profile of C III $\lambda 1909$ never does.

We have measured the value of v_{black} for all saturated absorption profiles mentioned above (these measurements are given in roman type in Table 4). For unsaturated absorption profiles (including, in the case of WR binaries, profiles which do not reach zero intensity because of the presence of a residual O star continuum), we have measured the velocity at the deepest point in the absorption profile (given in italics in Table 4). If a flat-bottomed but unsaturated profile is present, we measured the blueward edge of the flat region. These velocities are parenthesized in Table 4.

Figures 4a, 4b, and 4d show examples of the velocities measured in the profiles of C III $\lambda 1247$, C II $\lambda 1335$, and C III $\lambda 1909$

TABLE 3

MEAN AND RANGE OF OB STAR TERMINAL VELOCITIES AS A FUNCTION OF SPECTRAL TYPE AND LUMINOSITY CLASS

SPECTRAL TYPE	I			III			V		
	\bar{v}_{∞} (km s ^{−1})	Range (km s ^{−1})	N ^a	\bar{v}_{∞} (km s ^{−1})	Range (km s ^{−1})	N ^a	\bar{v}_{∞} (km s ^{−1})	Range (km s ^{−1})	N ^a
O3.....	3150	...	1	3190	3035–3370	3
O4.....	2325	1880–2605	3	2950	2750–3305	5
O5.....	1885	...	1	2810	2615–3160	4	2875	2810–2925	4
O5.5.....	1960	...	1
O6.....	2300	...	1	2560	2390–2730	2	2570	1635–3065	12
O6.5.....	2180	1820–2420	3	2545	2300–3000	4	2455	2155–2835	10
O7.....	2055	1425–2420	4	2600	2485–2665	3	2295	1780–3015	10
O7.5.....	1980	...	1	2175	1580–2390	7	1975	1745–2390	3
O8.....	1530	955–2185	3	2125	...	1	1755	1250–2230	7
O8.5.....	1955	1575–2160	4	2255	...	1	1970	1625–2315	2
O9.....	1990	1500–2450	5	1875	800–2250	9	1500	1120–1925	7
O9.5.....	1765	1590–2010	7	1505	1275–1990	4
O9.7.....	1735	1400–1860	7
B0.....	1535	795–2005	11
B0.2.....	1215	...	1
B0.5.....	1405	850–1865	14
B0.7.....	1155	...	1
B1.....	1065	490–1465	20
B1.5.....	750	510–1190	4
B2.....	790	510–1160	7
B2.5.....	490	435–550	2
B3.....	590	405–830	5

^a Number of stars.

TABLE 4

MAXIMUM VELOCITIES AT WHICH THE ABSORPTION MINIMUM OCCURS IN THE STRONGEST STELLER WIND LINES OF WN AND WC STARS

HD	Spectral Type	SWP	C III 21175.7	N V 21238.8	C III 21247.4	C II 21334.5	Si IV 21393.8	Si IV 21402.8	C IV 21548.2	He II 21640.4	N IV 21718.6	C III 21908.7	Mean ^a (excluding C IV)
104994.....	WN3	7020	...	3120
187282.....	WN4	15101	...	2290	2270	1785	(1750)	...	1940
65865.....	WN4.5	29703	1475	1345	1400	...	1375
190918.....	WN4.5 + O9.5 Ib	14715	...	1565	(1510)	(1425)	1560	...	1515
50896.....	WN5	(HP) ^b	...	1725	(1635)	(1580)	(1620)	...	1670
193077.....	WN5 + abs	15641	...	(1230)	1230	1195	1345	...	1220
193576.....	WN + O6	26007	...	1250	1785	...	1475
143414.....	WN6	16976	...	1575	1600	1590	1325	...	1480
191765.....	WN6	4088	...	1910	1795	1770	1905	...	1795
192163.....	WN6	30793	...	(1380)	1570	1565	1605	...	1545
211853.....	WN6 + O	14143	...	1150	(1465)	(1485)	1785	...	1450
62910.....	WN6-C4	27473	1530	1555	1600	...	1505
151932.....	WN7	4334	...	1550	1400	1380	1365	...	1335
92740.....	WN7 + abs	27342	1770	1790	1050	...	1510
93131.....	WN7 + abs	27341	...	(2325)	2130	2040	2155	...	1985
93162.....	WN7 + abs	15025	2105	2010	2455	...	1865
214419.....	WN + O	13996	1680	1440	1690	...	1340
86161.....	WN8	13893	...	(770)	755	755	(835)	...	720
96548.....	WN8	6927	...	955	955	920	(975)	...	930
115473.....	WC5	15105	2440	3025	2830	3225	...	2765
165763.....	WC5	2872	(2495)	2400	2405	2415	...	2330
76536.....	WC6	10113	(2450)	2080	2070	2055	...	2095
92809.....	WC6	15558	(2380)	2220	2250	2280	...	2240
119078.....	WC7	20280	1715	...	(1845)	1820	1850	1785	1850	1785	1750
156385.....	WC7	15130	2255	(2040)	2185	2100	2045	2100
97152.....	WC7 + O5-7	15107	1625	...	1910	1555	1750	1670	1645	1670
152270.....	WC7 + O5-8	15129	2185	...	(2130)	(2150)	2300	2310	2270	2190
192641.....	WC7 + O5	31507	1760	1680	1820	1920	1885	1830
193793.....	WC7 + O4-5	31504	(2600)	1510	2635	2900	2430
192103.....	WC8	22861	1505	...	1300	(1495)	1480	1460	1405	1420
68273.....	WC8 + O9 I	3377	1520	...	(1040)	1045	1415	1405	1415	1265
168206.....	WC8 + O8-O9 IV	34037	1715	1820	1885	1890	1720
136488.....	WC9	13816	1275	1140	(1120)	1160	1160
157451.....	WC9	16835	1300	1125	1095	1070	1130
164270.....	WC9	8156	1130	1190	1140	1025	1090	1060

NOTE.—Measurements of v_{blue} are indicated by values in roman type, the velocities of the deepest points in unsaturated absorption profiles are in italics, and the blueward edge of flat regions in unsaturated profiles are enclosed in parentheses.

^a “Mean” values in this column exclude the C IV values, to facilitate comparison between the two measures.

^b Values measured using the mean spectrum constructed by Howarth and Phillips 1986.

in the spectrum of the WC8 + O9 I binary γ Velorum. This spectrum (SWP 3377), obtained and first illustrated by Kondo, Feibelman, and West (1982), was taken at phase 0.534 (WC8 star in front), so that the orbital radial velocities of the component stars are minimized. The C IV $\lambda 1550$ profile (Fig. 4c) shows evidence of the winds from both components. We identify the black absorption edge velocity of -1415 km s^{-1} (*short vertical arrow*) with the wind of the WC8 component; this value is close to the velocities measured for the C III lines (Table 4), which can arise from only the WC8 wind. It agrees well with the terminal velocity of $1520 \pm 200 \text{ km s}^{-1}$ determined by Barlow, Roche, and Aitken (1988) for γ Vel from the profile of the $12.8 \mu\text{m}$ [Ne II] emission line, which is formed far out in the wind. The velocity of 2370 km s^{-1} which we identify with v_{back} for the O9 I component is indicated by the long vertical arrow in Figure 4c; it does not reach zero intensity because the O star wind does not absorb the WC8 continuum in the composite spectrum (the composite C IV profile is black as far as -1415 km s^{-1} because the absorption profiles of both stars are black as far as this velocity). With this interpretation, the C IV profile shown in Figure 4c implies that at 1540 \AA the

O9 I star continuum is 0.7 ± 0.2 mag brighter than that of the WC8 star. The implied terminal velocity of the O star falls within the range found for single O9 supergiants (Table 3).

Other WR binaries where we see evidence for a composite C IV profile are the WC7 binaries HD 87152, HD 152270, and HD 192641, for which we estimate O star wind terminal velocities of 2460, 2900, and 2750 km s^{-1} , respectively.

The *IUE* spectrum (SWP 26007) chosen for V444 Cyg (=HD 193576) came from the study of Shore and Brown (1988) and corresponds to phase 0.997 (WN5 star in front) so that, as with γ Vel, orbital motions relative to the observer are minimized. The *IUE* SWP images chosen for the spectroscopic binaries HD 190918 and HD 211853 were taken at phases 0.93 and 0.98, respectively.

Table 5 lists the values of v_{edge} and v_{back} ($=v_{\infty}$) that were measured for each of the Wolf-Rayet stars from their saturated C IV absorption profiles, except (d) for the case of the WN3 star HD 104994, where C IV $\lambda 1550$ is undetectable and we instead used N V $\lambda 1240$, and (b) for the case of the three WC9 stars, for which we adopted the velocities measured from C II $\lambda 1335$, since C⁺ is the dominant ion in the spectra of these stars.

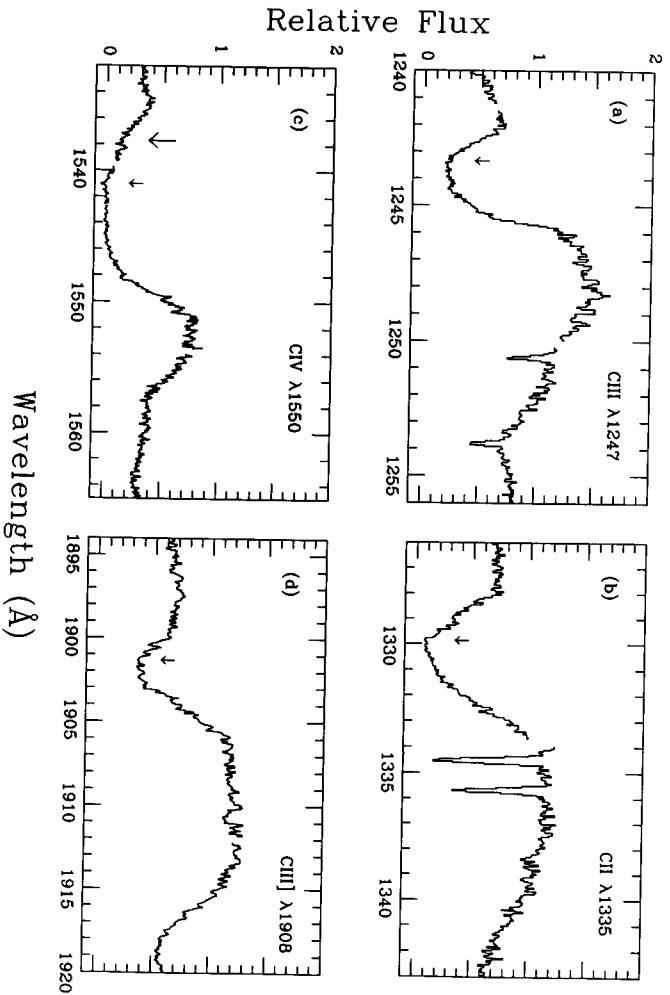


FIG. 4.—Examples of carbon line stellar wind profiles for HD 68273 (γ Vel; WC8 + O9 I). The maximum wind velocities at which the absorption minimum occurs in the WR wind (short arrow) and O star wind (long arrow) are indicated.

TABLE 5
STELLAR WIND VELOCITIES AND MASS-LOSS RATES FOR WR STARS

HD	WR*	SWP	Spectral Type	$v_{\text{edge}}^{\text{a}}$ (km s^{-1})	v_{∞}^{b} (km s^{-1})	$\log(\dot{M})$ ($M_{\odot} \text{ yr}^{-1}$)
104994.....	46	7020	WN3	3235	3120	...
187282.....	128	15101	WN4	2515	2270	...
65865.....	10	29703	WN4.5	2035	1475	...
190918.....	133	14715	WN4.5 + O9.5 Ib	1770	1625	-4.52
50896.....	6	(HP)	WN5	3140	1720	-4.12
193077.....	138	15641	WN5 + abs	1650	1345	-4.73
193576.....	139	26007	WN5 + O6	2325	1785	-4.62
143414.....	71	16976	WN6	2880	1590	...
191765.....	134	4088	WN6	2775	1905	-4.13
192163.....	136	30793	WN6	2700	1605	-4.02
211853.....	153	14143	WN6 + O	1900	1785	...
62910.....	8	27473	WN-C4	2540	1600	...
151932.....	78	4334	WN7	2125	1365	-4.31
92740.....	22	27342	WN7 + abs	2250	1790	...
93131.....	24	27341	WN + abs	2700	2155	...
93162.....	25	15025	WN7 + abs	3130	2455	...
214419.....	155	13996	WN7 + O	1920	1690	< -4.61
86161.....	16	13893	WN8	1000	855	...
96548.....	40	6927	WN8	1215	975	...
115473.....	52	15105	WC5	4250	3225	...
165763.....	111	2872	WC5	3500	2415	-4.50
76536.....	14	10113	WC6	2850	2055	...
92809.....	23	15558	WC6	3400	2280	...
119078.....	57	20280	WC7	2300	1770	...
156385.....	90	15130	WC7	2450	2045	< -4.46
97152.....	42	15107	WC7 + O5-7	2850	1645	...
152270.....	79	15129	WC7 + O5-8	3300	2270	-3.98
192641.....	137	31507	WC7 + O5	2550	1885	-4.48
193793.....	140	31504	WC7 + O4-5	3200	2900	-4.10
192103.....	135	22861	WC8	1920	1405	-4.36
68273.....	11	3377	WC8 + O9 I	1680	1415	-4.09
168206.....	113	34037	WC8 + O8-O9 IV	2025	1890	< -4.38
136488.....	69	13816	WC9	1615	1275	...
157451.....	92	16835	WC9	1870	1300	...
164270.....	103	8156	WC9	1310	1190	< -4.54

* Numbers from the catalog of van der Hucht *et al.* 1981.

The final column in Table 4 lists the mean of the absorption velocities, excluding C iv, measured for each WR star. Comparison of these mean velocities with the C iv velocities (which we generally adopt as v_∞) shows agreement to within 120 km s⁻¹ for 13 out of 16 WC stars and for 10 out of 19 WN stars. When present, the velocities given by the N v and Si iv resonance lines show good agreement with the C iv velocities. In the case of the WC stars, the C iii λ 1175 and λ 1247 excited state line velocities and the C ii resonance line velocities are in general agreement with the C iv velocities.

Hillier (1989) has suggested that the line-center optical depth of C iv λ 1550 can be so large ($\sim 10^9$) in the winds of WC stars that broad Lorentzian wings will affect its profile. However, we interpret the fact that the C iv black absorption edge velocities measured by us for the WC stars agree so well with the velocities measured from the Si iv, C ii, and C iii lines (Table 4) as indicating that Lorentzian damping wings do not significantly affect the position of the C iv black absorption edge in the spectra of these stars (or that all these lines have similar optical depths, which seems unlikely).

Single Wolf-Rayet stars are, in general, not observed to exhibit NACs in their UV P Cygni profiles (e.g., St-Louis, Willis, and Smith 1988), presumably because the UV resonance line absorption profiles in their spectra are almost always saturated. Some WR stars in spectroscopic binary systems have, however, been observed to exhibit NACs in their UV resonance line profiles. This phenomenon could be due to absorption of the companion O star continuum by the WR wind at large radii. Fitzpatrick, Savage, and Sitko (1982) observed an NAC in the Si iv profile of the WR binary HD 193793, with a central velocity of 2700 km s⁻¹ and a HWHM of 125 km s⁻¹, which was stable in velocity and strength over a period of 5 months. The terminal wind velocity of 2825 km s⁻¹ given by these data is consistent with the value of 2900 km s⁻¹ implied for the WC7 star by the C iv black absorption edge (Table 5). In the C iv and Si iv profiles of the WR binary HD 193077, Koenigsberger and Auer (1987) found absorption features at -1250 km s⁻¹, with widths of ~ 200 km s⁻¹. The implied terminal velocity of ~ 1350 km s⁻¹ is again consistent with the value of 1345 km s⁻¹ listed in Table 5.

c) Comparison with Other Estimates of v_∞

Groenewegen, Lamers, and Pauldrach (1989) have recently derived terminal velocities for the winds of 26 O stars, plus the B0 supergiant ϵ Ori, from *IUE* observations of resonance line profiles. They used a profile-fitting method which incorporates a turbulence parameter and therefore also derived terminal velocities significantly lower than v_{\max} . Their values show good agreement with those derived here (Table 1): the mean ratio (ours/theirs) is 0.97 ± 0.11 .

For the 10 WR stars in common, our values of v_{edge} (Table 5) show agreement with those measured by Willis (1982; his " v_a "). On the other hand, there is no simple correspondence between his "centre of the violet-displaced absorption component," v_0 , and the absorption velocities listed in Table 4.

Hillier (1987b) deduced a maximum flow velocity of 1600–1700 km s⁻¹ in the line formation region of the WN5 star HD 50896 from detailed modeling of the UV, optical, and IR line profiles, and he was forced to invoke a further acceleration of the wind at much larger radii in order to explain the much higher UV violet absorption edge velocities. (Hamann, Schmutz, and Wessolowski 1988 also reached this conclusion.) However, the terminal velocity of 1720 km s⁻¹ given by the

black absorption edge of C iv in the mean spectrum of Howarth and Phillips (1986; our Table 5) effectively eliminates the need to invoke further wind acceleration at large radii.

Torres, Conti, and Massey (1986) estimated wind terminal velocities for a large sample of WC stars by fitting the profiles of optical emission lines and extrapolating a line width versus excitation potential (EP) diagram to zero EP. For the 13 stars in common we find that their method gives velocities that are larger than the terminal velocities listed in Table 5 by an average factor of 1.21 ± 0.17 .

Williams and Ekenens (1989) have recently measured the velocities of the He i 2.058 μ m violet-displaced absorption line in the spectra of eight Wolf-Rayet stars and have argued that the absorption occurs far out in the winds, so that the velocities are representative of the wind terminal velocities. Of the five stars in common with our data, four give agreement to better than 80 km s⁻¹ between the values of v_∞ listed in Table 5 and the values of v_e (the central absorption velocity v_0 + HWHM) that they measured from the He i 2.058 μ m absorption profiles. The fifth object is the WN7 + O system HD 214419, for which our value of $v_\infty = 1690$ km s⁻¹ exceeds by 700 km s⁻¹ that for v_e measured by Williams and Ekenens.

Schmutz, Hamann, and Wessolowski (1989) have estimated wind terminal velocities for 30 WR stars from profile fits to (or, in some cases, from the observed maximum line widths of) He i and He ii emission-line profiles in the 0.5–1.1 μ m spectral region. There are 20 stars in common with our WR sample. For the five WC stars in common, the velocities derived by Schmutz *et al.* are a factor of 1.22 ± 0.11 larger than those given by the C iv λ 1550 black absorption edge (as discussed earlier, the velocities obtained from the Si iv, C ii, and C iii UV absorption profiles in WC star spectra are in agreement with those derived from C iv; Table 4). The eight WN4.5, WN5, WN6, and WN8 stars in common show good agreement between the terminal velocities derived by Schmutz *et al.* from the 0.6–1.1 μ m line widths and the terminal velocities derived here (the mean ratio is 1.00 ± 0.08). However, the velocities derived by Schmutz *et al.* for the four WN7 stars in their sample, and for the WN3 and WN4 stars HD 104994 and HD 187282, are much smaller than the terminal velocities derived here (the mean ratio is 0.65 ± 0.14). These stars have the weakest emission lines in their WR sample, and we interpret the above discrepancy as implying that the 0.6–1.1 μ m helium emission line width fits of Schmutz *et al.* do not yield the terminal velocity in the case of these weak-lined WR stars. This conclusion also appears to apply to the 2.058 μ m He i absorption profile measured by Williams and Ekenens (1989) in the spectrum of the WN7 system HD 214419 (see above).

IV. DISCUSSION

Figure 5 shows a plot of v_{edge} versus v_∞ for the O stars, B supergiants, and WR stars in our sample. For given values of v_∞ , the WR stars can be seen to have systematically higher values of v_{edge} . The WR stars have significantly ($\sim 10 \times$) higher rates of mass loss, \dot{M} , suggesting the possibility of a causal relationship, which we now investigate.

The last column of Table 5 lists mass-loss rates for those Wolf-Rayet stars in our sample which have been observed at radio wavelengths. Since the major WR radio survey by Abbott *et al.* (1986), a number of effects have been noted which lead to changes in their derived mass-loss rates.

1. Van der Hucht, Cassinelli, and Williams (1986) showed

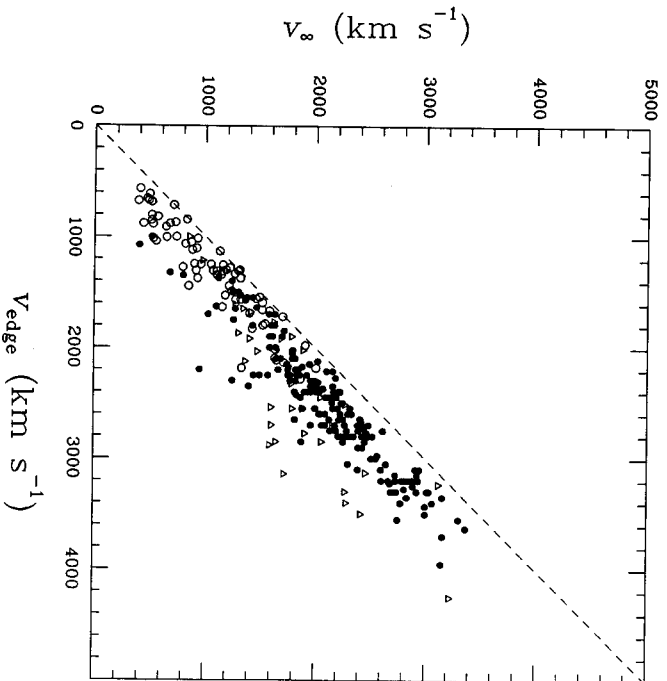


FIG. 5.—The terminal velocities of O (filled circles), B supergiant (open circles), and WR stars (open triangles) as a function of the maximum velocity observed in absorption in C IV, v_{∞} . The dashed line indicates the 1:1 relation for comparison.

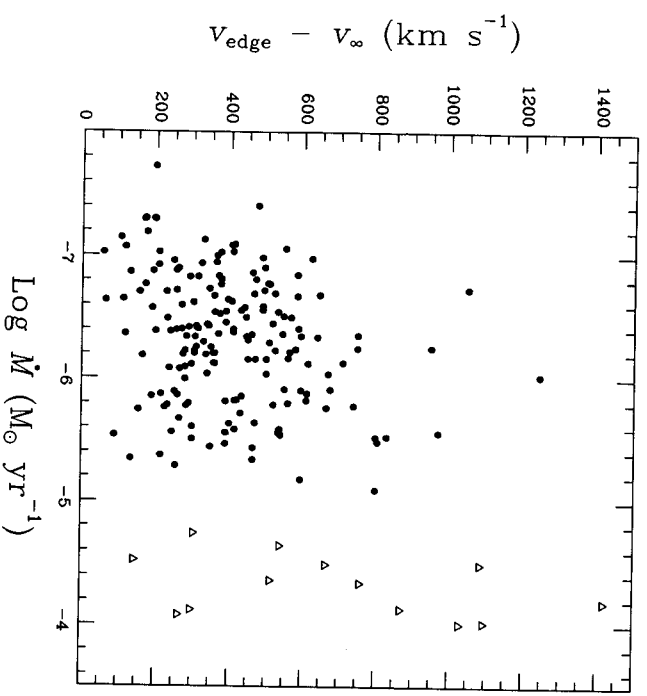


FIG. 6.— $v_{\infty} - v_{\infty}^{\text{edge}}$ as a function of mass-loss rate for O (filled circles) and WR (open triangles) stars.

that allowance for the high abundance of carbon in WC winds leads to an upward revision of the mass loss rates.

2. The ionization in WR winds has been predicted to decrease outward, such that the dominant ion at radio-emitting radii would be He^+ rather than He^{2+} (Schnitz and Hamann 1986; Hillier 1987a). This also leads to an upward revision of the mass-loss rates.

3. A reduction in the adopted wind terminal velocities (this paper) leads to a reduction in the derived mass-loss rates which is proportional to v_{∞} .

4. Very small (random) changes in the mass-loss rates are introduced by using distances from van der Hucht *et al.* (1988). (For HD 50896 we adopted $D = 2$ kpc, after Howarth and Phillips 1986).

The WR mass-loss rates listed in Table 5 have been derived using the formula of Wright and Barlow (1975) and the radio fluxes, or upper limits, measured by Abbott *et al.* (1986), Hogg (1982; for HD 214419), Becker and White (1985; the "low" state flux for HD 193793) and Hogg (1989; for HD 50896, 151932, 152270, 191765, and 192163). A temperature of 6000 K was adopted for the radio-emitting regions (Hogg 1985). For the WN stars, He^+ was assumed to be the dominant ion, except for the cases of HD 151932 and HD 193077, where we adopted $\text{H}^+/\text{He}^+ = 1$ and 1.6, respectively (Conit, Leep, and Perry 1983; Schnitz, Hamann, and Wessolowski 1988). For the WC stars we adopted $\text{C}^2/\text{He}^+ = 0.3$ (Smith and Hummer 1988; Torres 1988). The mass loss rates listed in Table 5 assume the same wind terminal velocity in all directions from the WR star. Poe, Friend, and Cassinelli (1989) have proposed that WR stars may have lower terminal velocities and high densities in their equatorial zones, thereby reducing the mass-loss rates that should be derived from the observed radio fluxes.

Figure 6 shows the plot of $(v_{\infty} - v_{\infty}^{\text{edge}})$ versus $\log \dot{M}$ for the O

stars and WR stars in our sample. The O star mass-loss rates are those listed in Table 10 of Howarth and Prinja (1989), which include a statistical correction for the average effect of revised terminal velocities. A loose correlation ($r = 0.36$) between \dot{M} and the excess absorption velocity ($v_{\infty}^{\text{edge}} - v_{\infty}$) is present in the data shown in Figure 6. To quantify this effect further, Table 6 lists the mean values of $v_{\infty}/v_{\infty}^{\text{max}}$ found for O V, O III, O I, B I, and WR stars. The mean value of $v_{\infty}/v_{\infty}^{\text{edge}}$ is found to decrease steadily from 0.88 for O V stars, 0.84 for O III and O I stars, through to 0.80 for O I and B I stars and 0.76 for WR stars. This is also a sequence of generally increasing C^{3+} column density. We interpret this trend in terms of two effects. First, among the O stars, the supergiants, which have higher mass-loss rates than the dwarfs or giants, tend to have lower terminal velocities (Table 3). If the amplitude of high-velocity perturbations in the wind was independent of the final terminal velocity reached, this might contribute part of the effect. Probably more important is the fact that the highest velocity material in an unstable radiatively driven wind is predicted to be extremely rarefied. In a low-density wind, such material would be unlikely to have enough optical depth to be seen in absorption, whereas a high mass-loss rate would lead to larger

TABLE 6
RATIO OF v_{∞} TO v_{∞}^{edge} AND v_{∞}^{max}

Spectral Type	Number	$v_{\infty}/v_{\infty}^{\text{edge}}$	$v_{\infty}/v_{\infty}^{\text{max}}$
O I	39	0.80 ± 0.08	2.60 ± 0.38
O II	11	0.84 ± 0.06	2.75 ± 0.51
O III	35	0.84 ± 0.06	2.41 ± 0.47
O3 V-O7 V	45	0.87 ± 0.05	2.26 ± 0.37
O7.5 V-O9 V	19	0.89 ± 0.04	1.67 ± 0.44
O N	5	0.69 ± 0.15	1.38 ± 0.34
OIf	5	0.70 ± 0.16	1.98 ± 0.52
B0-I-B3 I	65	0.80 ± 0.13	1.96 ± 0.60
WR	35	0.76 ± 0.12	...

NOTE.—Quoted errors are standard deviations.

absorption and a greater probability for the highest velocity material to be detectable.

We note that the present results do not significantly change the overall *slope* of the \dot{M} versus L relation for OB stars, as determined by previous workers. Radio mass-loss rates (which scale as v_∞) have been obtained mainly for supergiants and so (from Table 6) should decrease by a mean factor of 0.80. UV-based mass loss rates (which scale as v_∞^2) have been derived mainly for samples of dwarfs and giants and so (from Table 6) should decrease by a mean factor of $(0.88)^2 = 0.77$. Thus the overall slope found for composite radio-UV samples should be unchanged, although the scale factor should be decreased by ~ 0.8 . (This change in the scaling constant is already included in the mass-loss rates given by Howarth and Prinja 1989.)

Starting with Snow and Morton (1976) and Abbott (1978), the terminal wind velocities of OB stars have often been compared with their escape velocities, v_{esc} . In Figure 7 we plot the wind terminal velocities derived for the O stars in our sample against the escape velocities derived for them by Howarth and Prinja (1989); different symbols have been assigned to dwarfs, giants, and supergiants. The peculiar stars HD 37022 and HD 93521 have been excluded from this diagram.

The 70 B0–B3 supergiants in our sample are also plotted in Figure 7. Their escape velocities have been derived from the stellar parameters tabulated by Leitherer (1988) and are listed in Table 2 (where individual values of v_{esc} were not available, we adopted the mean value, indicated by parentheses, for the appropriate spectral subclass). Table 6 lists the mean values of $(v_\infty/v_{\text{esc}})$ found for each of these groups. This ratio is found to increase from 1.7 for the late O dwarfs to 2.4 for the O giants and 2.6 for the O supergiants. The mean ratio found for all 151 O stars with assigned luminosity classes (but excluding Op, Oe, ON, and OC stars) is $v_\infty/v_{\text{esc}} = 2.36 \pm 0.51$. This compares

with the ratio of 2.78 ± 0.36 derived for the 27 stars in their sample by Groenewegen, Lamers, and Pauldrach (1989). The latter authors have discussed possible reasons for the discrepancy between observed ratios of v_∞/v_{esc} and the value of 3.9 they obtain for radiation pressure-driven wind models.

The 249 stars plotted in Figure 7 (which excludes HD 93521 and HD 37022; § IIIa) yields a correlation coefficient of $r = 0.76$, while a least-squares fit to the data gives $v_\infty = (74 \pm 101) + (2.145 \pm 0.182)v_{\text{esc}}$. [or alternatively $v_{\text{esc}} = (333 \pm 29) + (0.266 \pm 0.015)v_\infty$]. The OB supergiants alone yield a correlation coefficient of $r = 0.83$.

Inspection of the mean values of v_∞/v_{max} listed in Table 6 reveals that the five Ofp stars in the sample have a low mean ratio of 0.70. Since, as discussed above, this ratio appears to decrease with increasing mass-loss rate, this behavior is consistent with the Ofp stars having higher mass-loss rates than other O stars. The mean value of v_∞/v_{esc} for the Ofp stars (1.98) is also significantly lower than found for the normal O stars. This may be due to the Ofp stars having already lost a large fraction of their original mass, with their current masses (and hence escape velocities) being overestimated by evolutionary track fitting. While there is a steady increase in v_∞/v_{esc} from 2.1 for the O V stars to 2.75 for the O II stars (Table 6), there is also a decrease in this quantity to 2.6 for the O I stars, suggesting the possibility that the higher mass-loss rates of this group again lead to lower masses, and therefore lower escape velocities, than predicted by the evolutionary tracks.

We find the interesting result that the five ON stars in our

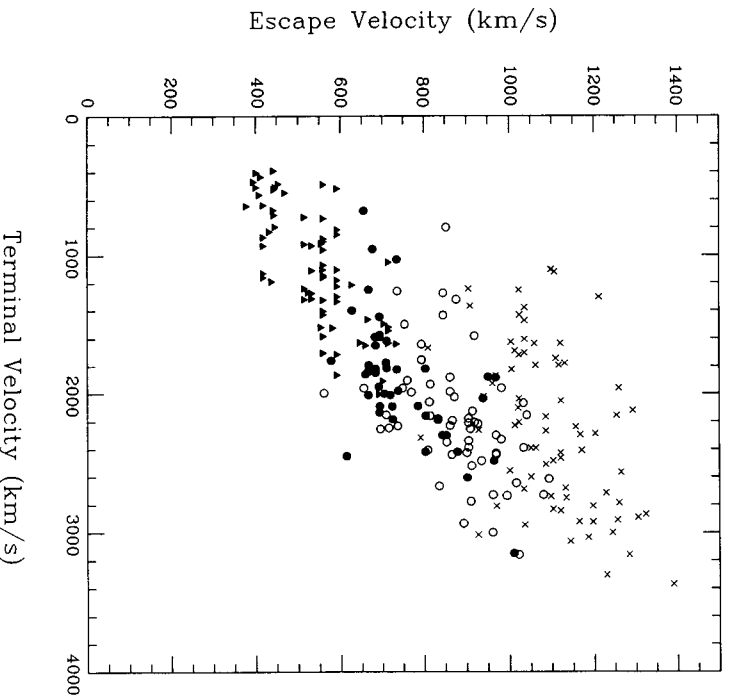


Fig. 7.—The photospheric escape velocity (see text for sources) versus the wind terminal velocity for B type supergiants (filled triangles), O type supergiants (filled circles), O type giants (open circles), and O type dwarfs (crosses).

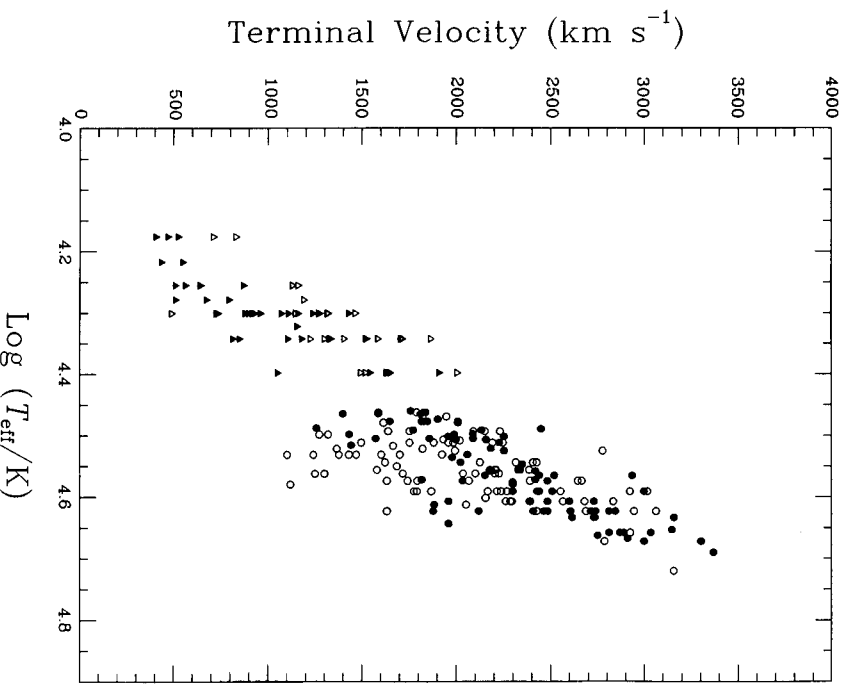


Fig. 8.—The terminal velocity as a function of effective temperature. The terminal velocities were derived from $v_{\text{H}\alpha}$ and $v_{\text{H}\alpha} + \text{HWHM}_{\text{H}\alpha}$ for O stars (filled and open circles, respectively) and B supergiants (filled and open triangles, respectively).

sample (three dwarfs and two supergiants) yield low mean values for both v_{∞}/v_{\max} (0.69) and $v_{\infty}/v_{\text{esc}}$ (1.38; Table 6). The three ON dwarf stars all have spectral types between O7 and O9. The mean value of $v_{\infty}/v_{\text{esc}}$ for normal O dwarfs within this spectral type range is also low (1.67, Table 6), but the normal late O dwarfs have a mean value for v_{∞}/v_{\max} of 0.89, significantly higher than found for the ON dwarfs. The ON stars might have physical parameters that are significantly different from those implied by their nominal spectral types. Schönberner *et al.* (1988) found that nitrogen was strongly enhanced in the atmospheres of a number of OBN main-sequence stars and discussed a variety of scenarios which might have led to this situation. For one of the stars, HD 14633 (ON8 V), their spectroscopically derived value of $\log g = 3.70$ is more like that expected for a giant than a main-sequence star and is 0.26 dex lower than the value derived from the parameters implied by its spectral type that are given by Howarth and Prinja (1989). If the mass and escape velocity of HD 14633 were correspondingly lowered, then the anomaly of its small value of $v_{\infty}/v_{\text{esc}}$ would disappear. Strong mixing, possibly rotationally induced, may lead to evolutionary tracks for ON stars near the main sequence quite unlike those for normal O stars (Maeder 1987), and hence the masses (and $\log g$ and v_{esc} values) estimated from evolutionary tracks could be in error. However, the reason for the low values found for the purely empirical ratio v_{∞}/v_{\max} in the case of the ON stars is not obvious, unless these stars have much higher mass loss rates than hitherto suspected.

REFERENCES

- Abbott, D. C. 1978, *Ap. J.*, **225**, 893.
 ———, 1985, in *Progress in Stellar Line Formation Theory*, ed. J. E. Beckman and L. Crivellari (Dordrecht: Reidel), p. 279.
 Abbott, D. C., Bieging, J. H., Churchwell, E., and Torres, A. V. 1986, *Ap. J.*, **303**, 239.
 Barlow, M. J. 1989, in *IAU Symposium 131, Planetary Nebulae*, ed. S. Torres-Peimbert (Dordrecht: Kluwer), p. 319.
 Barlow, M. J., and Cohen, M. 1977, *Ap. J.*, **213**, 737.
 Barlow, M. J., Roche, P. F., and Aitken, D. K. 1988, *M.N.R.A.S.*, **232**, 821.
 Becker, R. H., and White, R. L. 1983, *Ap. J.*, **297**, 649.
 Castor, J. I., and Lamers, H. J. G. L. M. 1979, *Ap. J. Suppl.*, **39**, 481.
 Conti, P. S., Leep, E. M., and Perry, D. N. 1983, *Ap. J.*, **268**, 228.
 Fitzpatrick, E. L., Savage, B. D., and Sliko, M. L. 1982, *Ap. J.*, **256**, 578.
 Groenewegen, M. A. T., Lamers, H. J. G. L. M., and Pauldrach, A. W. A. 1989, *Astr. Ap.*, **221**, 78.
 Hamann, W.-R. 1980, *Astr. Ap.*, **84**, 342.
 ———, 1981, *Astr. Ap.*, **93**, 353.
 Hamann, W.-R., Schmutz, W., and Wessolowski, U. 1988, *Astr. Ap.*, **194**, 190.
 Heap, S. R. 1982, in *Advances in Ultraviolet Astronomy* (NASA CP-2238), p. 562.
 Heck, A., Egnel, D., Jaschek, M., and Jaschek, C. 1984, *IUE Low Dispersion Spectral Atlas* (ESA SP-1052).
 Hennrichs, H. F., Kaper, L., and Zwarthoed, G. A. A. 1988, in *A Decade of UV Astronomy with the IUE Satellite* (ESA SP-281), Vol. 2, p. 145.
 Hillier, D. J. 1987a, *Ap. J. Suppl.*, **63**, 947.
 ———, 1987b, *Ap. J. Suppl.*, **63**, 965.
 ———, 1989, *Ap. J.*, **347**, 392.
 Hiltner, W. A. 1956, *Ap. J. Suppl.*, **2**, 389.
 Hogg, D. E. 1982, in *IAU Symposium 99, Wolf-Rayet Stars: Observations, Physics, Evolution*, ed. C. W. H. de Loore and A. J. Willis (Dordrecht: Reidel), p. 221.
 ———, 1985, in *Radio Stars*, ed. R. M. Hjellming and D. M. Gibson (Dordrecht: Reidel), p. 117.
 ———, 1989, *Pub. A.S.P.*, **98**, 282.
 Howarth, I. D. 1984a, *M.N.R.A.S.*, **206**, 625.
 ———, 1984b, *M.N.R.A.S.*, **211**, 167.
 Howarth, I. D., and Phillips, A. P. 1986, *M.N.R.A.S.*, **222**, 809.
 Howarth, I. D., and Prinja, R. K. 1989, *Ap. J. Suppl.*, **69**, 527.
 Koenigberger, G., and Auer, L. H. 1987, *Rev. Mexicana Astr. Af.*, **14**, 271.
 Kondo, Y., Feibelman, W. A., and West, D. K. 1982, *Ap. J.*, **252**, 208.
 Lamers, H. J. G. L. M., Gahler, R., and Snow, T. P. 1982, *Ap. J.*, **258**, 186.
 Leitherer, C. 1988, *Ap. J.*, **326**, 356.
 M. J. Barlow, I. D. Howarth, and R. K. Prinja: Department of Physics and Astronomy, University College London, G. Street, London WC1E 6BT, England, UK
 [SPAN:19457::ZUVAD::MJB, IDH, RKP;
 Bitnet: MJB, IDH, RKP@STAR.UCL.AC.UK]
 Lesh, J. R. 1968, *Ap. J. Suppl.*, **16**, 371.
 Lucy, L. B. 1982, *Ap. J.*, **255**, 278.
 ———, 1983, *Ap. J.*, **274**, 372.
 Maeder, A. 1987, *Astr. Ap.*, **178**, 159.
 Morgan, W. W., Code, A. D., and Whitford, A. E. 1956, *Ap. J. Suppl.*, **2**, 41.
 Morton, D. C. 1976, *Ap. J.*, **203**, 386.
 Owocki, S., Castor, J. I., and Rybicki, G. B. 1988, *Ap. J.*, **335**, 914 (OCR).
 Pauldrach, A. W. A., Puls, J., Kudritzki, R. P., Mendez, R. H., and Heap, S. R. 1988, *Astr. Ap.*, **207**, 123.
 Poe, C. H., Friend, D. B., and Cassinelli, J. P. 1989, *Ap. J.*, **337**, 888.
 Prinja, R. K. 1988, *M.N.R.A.S.*, **231**, 21P.
 ———, 1989, *M.N.R.A.S.*, **241**, 721.
 ———, 1990, *Astr. Ap.*, **232**, 119.
 Prinja, R. K., and Howarth, I. D. 1986, *Ap. J. Suppl.*, **61**, 357.
 ———, 1988, *M.N.R.A.S.*, **233**, 123.
 Prinja, R. K., Howarth, I. D., and Hennrichs, H. F. 1987, *Ap. J.*, **317**, 389.
 St-Louis, N., Willis, A. J., and Smith, L. J. 1988, in *A Decade of UV Astronomy with the IUE Satellite* (ESA SP-281), **2**, p. 125.
 Schmutz, W., and Hamann, W.-R. 1986, *Astr. Ap.*, **166**, L11.
 Schmutz, W., Hamann, W.-R., and Wessolowski, U. 1989, *Astr. Ap.*, **210**, 236.
 Schoenberner, D., Herrero, A., Becker, S., Eber, F., Butler, K., Kudritzki, R. P., and Simon, K. P. 1988, *Astr. Ap.*, **197**, 209.
 Shore, S. N., and Brown, D. N. 1988, *Ap. J.*, **334**, 1021.
 Smith, L. F., and Hummer, D. G. 1988, *M.N.R.A.S.*, **230**, 511.
 Snow, T. P. 1977, *Ap. J.*, **217**, 760.
 Snow, T. P., and Morton, D. C. 1976, *Ap. J. Suppl.*, **32**, 429.
 Stieckland, D. S. 1989, *Observatory*, **109**, 74.
 Torres, A. V. 1988, *Ap. J.*, **325**, 759.
 Torres, A. V., Conti, P. S., and Massey, P. 1986, *Ap. J.*, **300**, 379.
 Uesugi, A., and Fukuda, T. 1982, *Reisels Catalogue of Stellar Rotational Velocities* (Kyoto: Department of Astronomy, Kyoto University).
 van der Hucht, K. A., Cassinelli, J. P., and Williams, P. M. 1986, *Astr. Ap.*, **168**, 111.
 van der Hucht, K. A., Conti, P. S., Lundstrom, L., and Stenholm, B. 1981, *Space Sci. Rev.*, **28**, 227.
 van der Hucht, K. A., Hidayat, B., Admiranto, A. G., Supelli, K. R., and Doorn, C. 1988, *Astr. Ap.*, **199**, 217.
 van Genderen, A. M., *et al.* 1988, *Astr. Ap. Suppl.*, **74**, 467.
 Walborn, N. R., and Nichols-Bohlin, J. 1987, *Pub. A.S.P.*, **99**, 611.
 Williams, P. M., and Evers, P. R. J. 1989, *M.N.R.A.S.*, **240**, 445.
 Willis, A. J. 1982, *M.N.R.A.S.*, **198**, 897.
 Wright, A. E., and Barlow, M. J. 1975, *M.N.R.A.S.*, **170**, 41.

Finally, we note that although there is a good correlation ($r = 0.76$) between v_{∞} and v_{esc} (Fig. 7), as predicted by radiation pressure driven-wind models, for the present sample an even better correlation ($r = 0.86$) exists between v_{∞} and T_{eff} . Figure 8 shows a plot of terminal velocity versus T_{eff} for the O stars and B supergiants in our sample (we adopted the effective temperature scale of Howarth and Prinja 1989 for the O type stars, and the effective temperature scale of Barlow and Cohen 1977 for the B supergiants). Prinja (1990) has demonstrated that Be stars are also consistent with the trend shown in Figure 8. A similar trend to that shown in Figure 8 has been found for the central stars of planetary nebulae by Pauldrach *et al.* (1988). However, planetary nebula central stars exhibit a relatively narrow mass range ($0.60 \pm 0.02 M_{\odot}$; Barlow 1989) and during their hydrogen-shell burning phase evolve to higher effective temperatures at constant luminosity, so the dependence of v_{∞} upon T_{eff} is essentially the same as that upon v_{esc} . For the case of the OB stars plotted in Figure 8, a mass range as narrow as that found for planetary nebula central stars would be most unexpected.

We thank D. J. Stieckland for information about the orbital phases corresponding to the IUE images of HD 190918 and HD 211853 and N. R. Walborn for recommendations in respect of spectral types.